Catalysis Letters (2020) 150:3036–3048
https://doi.org/10.1007/s10562-020-03208-w

In Situ DRIFTS Investigation of Ethylene Oxidation on Ag and Ag/Cu on Reduced Graphene Oxide

Monique R. D'Oliveira[1] · Jessica Rabelo[1] · Amanda Garcez Veiga[2] · Carlos Alberto Chagas[3] · Martin Schmal[1,4]

Received: 19 December 2019 / Accepted: 3 April 2020 / Published online: 13 April 2020

Abstract

Reduced graphene oxide (rGO) was synthesized and impregnated with silver and silver/copper for in situ DRIFTS investigation of ethylene oxidation. The catalysts were characterized using different techniques. SEM micrographs showed that the metals are dispersed on the rGO surface. XPS results showed the presence of the metallic silver and copper as CuO and Cu_2O oxides. The in situ DRIFTS showed that in both catalysts the total oxidation of ethylene reaction prevails besides the intermediate formation of acetaldehyde. The presence of Cu ions or CuO and Cu_2O at the surface indicate the presence of electronic structure, which may enhance the oxidation reaction.

Electronic supplementary material The online version of this article (https://doi.org/10.1007/s10562-020-03208-w) contains supplementary material, which is available to authorized users.

Extended author information available on the last page of the article

Graphic Abstract

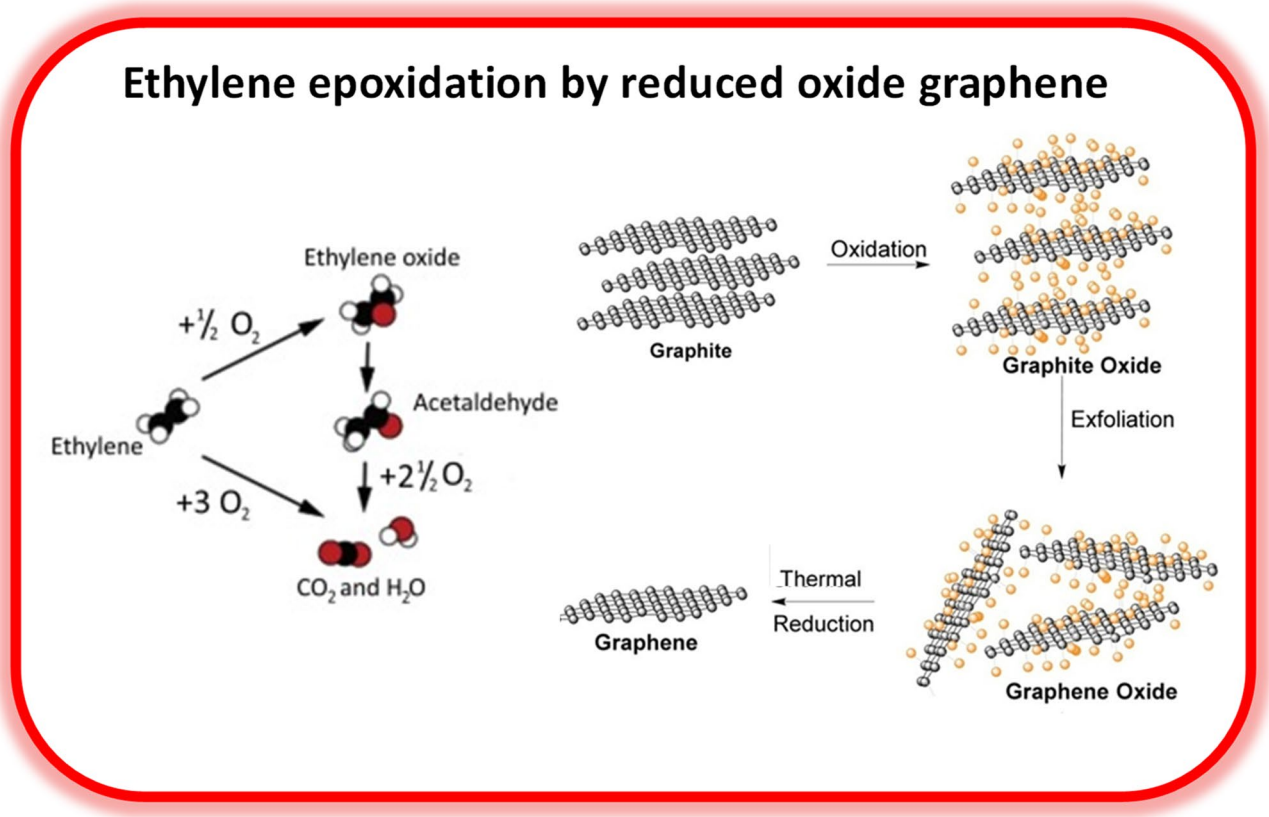

Keywords Reduced graphene oxide · Epoxidation of ethylene · Nanoparticles · Silver · Copper

1 Introduction

Ethylene oxide (EO) is one of the major derivatives of ethylene. Characterized by a special reactivity, ethylene oxide can generate a series of fine chemicals for a wide range of applications. The main use of ethylene oxide is in the production of ethylene glycol, the main constituent of engine coolants, and in other diols (or glycols), which are used to make polyesters [1]. A particularly important class of industrial reactions involves the selective oxidation of hydrocarbons over heterogeneous Ag-based catalysts. In terms of scale and market value, the epoxidation of ethylene to form ethylene oxide is by far the most important industrial catalytic process performed on Ag catalysts [2]. In the commercial process for ethylene oxide production, ethylene epoxidation is performed on silver catalysts. Since the discovery of this reaction by Lefort, significant efforts have been made to improve the catalysts used in this process [3]. The uniqueness of Ag as an ethylene epoxidation catalyst is due to: (i) Ag–O bond strength, (ii) chemical nature of adsorbed oxygen species, and (iii) inability of Ag–O to activate the C-H bond of ethylene [4]. Studies showed that atomic oxygen is the active species for the partial oxidation of ethylene. Thus, the catalyst should be able to dissociate the oxygen molecule, which can be easily achieved on the transition metals as well as by Ag and Cu. On metals that do not activate CH bonds, the surface oxygen has been found to act as a Lewis base that promotes C–H activation. In the case of ethylene, it has been proposed that this initiates total combustion [5].

The oxide surfaces are the active phase for the (partial) oxidation reactions. The presence of subsurface oxygen has been reported to increase catalyst selectivity even for the metallic surfaces. The electrophilic nature of bridging oxygen atoms on the Ag_2O surface makes them very selective for the epoxidation reaction and the possibility of a direct epoxidation pathway that proceeds through a low activation energy [2].

Silver and copper exhibit a synergy when alloyed together and used to catalyze ethylene epoxidation. The addition of a small amount (< 1%) of Cu to Ag catalysts gives rises to an increase in epoxide selectivity of about 50%. Metallic AgCu alloys should be more selective to epoxide because the energy

barrier to form epoxide should be lower than the barrier to form the aldehyde (which leads to total combustion) [7]. Bimetallic catalysts have been studied and applied in the ethylene epoxidation, with emphasis on catalysts based on copper and silver. Jankowiak and Barteau [6] studied the monometallic silver and bimetallic Ag–Cu catalysts, indicating that the bimetallic catalyst was more selective for the ethylene oxide formation when compared to pure silver catalyst. Greiner et al. [7] showed in their work that the unsupported alloy AgCu with copper (less than 1% by mass) favored the selectivity of the partial oxidation of ethylene, and that the cooper oxide is stable, compared to the silver oxide. They observed that copper segregated to form an oxide overlayer. The AgCu alloy exhibited higher ethylene oxide when compared to the isolated Ag and Cu.

Several catalysts based on graphene have been developed and applied in numerous catalytic reactions, such as oxygen reduction reaction (ORR) [8, 9], Fischer–Tropsch synthesis (FTS) [10, 11], CO_2 reduction [12, 13], water splitting [14, 15], selective hydrogenation [16–18], NO_x abatement [19–21], catalytic purification of VOCs [22, 23] and waste water treatment [20, 24]. According to Ramakrishnan et al. [25] because graphene has high surface area, unique graphitized plane and high electrical conductivity. Significant is that the addition of nitrogen atom into reduced graphene oxide (rGO) improves the catalytic activity because of the high electron-transport kinetics and the ability to prevent the agglomeration of nanoparticles on the substrate. The promising and exciting results make the graphene-based catalysts to be considered as the future revolutionary materials in catalysis [26].

Graphene is thus considered as one of the most promising materials in a wide range of applications [27–30]. Given the large specific surface area, two-dimensional structure, facile decoration and high adsorption capacity, its use has been extensively investigated in catalysis [27, 32]. The graphene can be used like active phase or as support for metals and metal oxides [29, 33, 34]. The structure characteristic makes graphene highly desirable for the potential application to act as a two-dimensional support for metallic nanoparticles with high dispersion [26, 35]. In addition, the local conjugate structure gives the graphene an improved adsorption capacity with respect to the substrates in the catalytic reaction [36]. In the present work, we present the synthesis and characterization of silver and silver/copper supported on graphene and the in situ DRIFTS analyses of the ethylene oxidation reaction.

2 Experimental Section

2.1 Materials

Graphite powder was supplied by Nacional de Grafite Ltda (Brazil). Potassium permanganate ($KMnO_4$) was purchased from SIGMA-ALDRICH. Concentrated sulfuric acid (H_2SO_4), hydrochloric acid (HCl), cupric nitrate tri-hydrate ($Cu(NO_3)_2.3H_2O$), silver nitrate ($AgNO_3$) and hydrogen peroxide (30 wt%) were purchased from VETEC Quimica Fina Ltda. All chemicals were used as received without any further purification.

2.2 Synthesis of Graphene Oxide

Graphene oxide (GO) was prepared from graphite, according to modified Hummer's method [37]. First, 12 g of graphite powder were dissolved into 280 mL of concentrated sulfuric acid solution under stirring speed of 500 rpm in ice bath. Then, 36 g of potassium permanganate was slowly added into the mixture under stirring, while the temperature was kept at lower than 20 °C and subsequently heated up to 40 °C for 2 h. Then, 600 mL of distilled water was added slowly, and the solution was heated to 95 °C under stirring for 15 min. Next, distilled water (2000 mL) was diluted to the mixture and then 60 mL of hydrogen peroxide was slowly added into the suspension under stirring (500 rpm), turning the color of the solution from dark brown to caramel. After that, the supernatant was decanted away and the solid obtained was then washed with water and diluted HCl (10%). The product GO was collected by centrifugation and washed with distilled water several times until neutral pH and finally dried at 60 °C for 24 h to produce the GO.

2.3 Synthesis of Reduced Graphene Oxide

The reduced graphene oxide (rGO) was prepared by the thermal method. The final GO was thermally treated under air flow up to 300 °C with a heating rate of 30 °C/min. The rapid temperature increase makes the oxygen-containing functional groups attached on carbon plane decompose into gases (CO_2 and CO) and water vapor [38]. The rapid release of these gases increases the internal pressure of the structure, resulting in exfoliation of graphite oxide, forcing the layers to separate. After exfoliation, a significant increase in solid volume occurs. Then, the temperature was increased up 500 °C under He flow and heating rate of 10 °C/min to obtain the reduced rGO.

2.4 Synthesis of Supported Ag and Ag–Cu/Reduced Graphene Oxide Catalysts

The Ag/rGO and Ag–Cu/rGO catalysts were synthesized by incipient wetness impregnation method. The solution of $AgNO_3$ was prepared and added slowly to the graphene (rGO) support. After impregnation, the sample was dried at 110 °C overnight, followed by calcination at 300 °C in nitrogen for 1 h. The catalyst was named as Ag/rGO. Subsequently, copper was impregnated over the Ag/rGO

catalyst, using $Cu(NO_3)_2.3H_2O$ as precursor salt, dried and calcined similarly. The nominal loadings of silver and copper were 10 and 5 wt%, respectively. The bimetallic catalyst was named as Ag–Cu/rGO.

2.5 Characterizations

X-ray powder diffraction (XRD) analysis was carried out in Rigaku Miniflex diffractometer in air at ambient conditions using CuK_α ($\lambda = 1.5406$ Å) as radiation source. The working voltage was 20 kV and the current of 15 mA. XRD data were collected in the 2θ range from 5 to 90° with 0.05° a step size and 1 s counting time per point in continuous scan mode. Crystal phases were identified by using JCPDS (Joint Committee on Powder Diffraction Standards) database. The mean crystallite sizes of different phases were estimated by using the Scherrer equation.

In order to characterize the thermal stability and the loading amount of metal dispersed in graphene, the thermogravimetric analysis (TGA) was carried out on a Hitachi equipment, model STA7300. TGA curves were obtained under nitrogen and air gas flow (80 mL/min) at a heating rate of 10 °C/min from 30 to 1000 °C.

Textural properties were obtained by N_2 adsorption/desorption isotherms at liquid nitrogen temperature (− 196 °C), using a Micromeritics ASAP2010 instrument. The samples were previously degassed under high vacuum at 200 °C overnight in order to remove adsorbed species. The specific surface area was calculated using the Brunauer–Emmett–Teller (BET) method in a relative pressure range of 0.05–0.3. The pore size distributions were determined from desorption branches by the Barrett–Joyner–Halenda (BJH) method.

The morphology and microstructure of the catalysts were examined using a QUANTA FEG 400 scanning electron microscope (SEM) with acceleration voltage of 30 kV and HELIOS NanoLab DualBeam G3 CX. Elemental mappings were obtained with energy dispersive X-ray spectroscopy (EDS) attached to SEM. For sample preparation, the powders were dispersed on a double-sided adhesive carbon tape, previously adhered in the sample holder. Scanning transmission electron microscopy (STEM) analysis were performed on JEOL 2100F at an accelerating voltage of 200 kV.

The surface chemical state of the atoms and their relative abundance were evaluated by X-ray photoelectron spectroscopy (XPS) using Escalab 250Xi Thermo Scientific spectrometer with a monochromatic AlK_α (1486.6 eV) X-ray source. The XP spectra were acquired at constant analyzer energy mode (CAE) with pass energy of 100 eV for survey and 25 eV for high resolution. The C 1 s signal at 284.6 eV was the binding energy reference.

2.6 In situ Diffuse Reflectance Infrared Fourier Transform Spectroscopy (DRIFTS)

DRIFTS measurements were performed on a Nicolet spectrometer (Nexus 470 model) equipped with a MCT detector cooled by liquid nitrogen. Before the measurement has been performed, the catalysts were pretreated under flowing mixture of 5 vol% O_2/He (30 ml/min) at 350 ºC (for Ag/rGO catalyst) and 280 ºC (for Ag–Cu/rGO catalyst) for 2 h [39].

After cooling down to room temperature, a background spectrum was collected for spectrum correction. Subsequently, the reaction mixture (20 vol% C_2H_4 + 5 vol% O_2 in He balance) was introduced in the DRIFTS cell at atmospheric pressure. The spectra were collected at 25, 100, 250, 300 and 400 °C (for Ag/rGO catalyst) and 25, 100, 240, 280 and 320 °C (for Ag–Cu/rGO catalyst) in the 3500–600 cm^{-1} range operating at a resolution of 4 cm^{-1}. Backgrounds were collected at desired temperatures after 10 min to allow equilibrium at that temperature. Difference spectra were obtained by subtracting the background from the subsequent spectra. KBr beam splitter was used to obtain spectra in the range of 3500–600 cm^{-1}.

3 Results and Discussion

Information about crystal structure and phase formation was obtained by XRD measurements [29, 40]. The XRD patterns of natural graphite and GO are illustrated in Fig. S1 (supplementary information, SI). The natural graphite exhibited a high crystalline degree with a strong and sharp peak about 2θ = 26° corresponding to (002) crystal planes with an interlayer spacing of 3.36 Å, indicating that the spatial arrangement of graphite crystal layers is extremely regular [41]. On the contrary, the crystalline degree of GO is relatively low with a broad peak about at 2θ = 11°, corresponding to an interlayer spacing of 8.32 Å. This increasing interlayer spacing is due to introduction of oxygen functional groups between graphite layers during the oxidation process [42].

XRD diffraction for catalysts and rGO support are shown in Fig. 1. All patterns showed a broad signal located at 2θ = 25.5° characteristic to rGO (002) crystalline plane of the hexagonal structure [43], corresponding to an interlayer distance of 3.47 Å. No remaining peaks of graphene oxide were observed, confirming successful reduction of GO to rGO. The Ag/rGO and Ag–Cu/rGO catalysts showed very similar XRD patterns, with peaks located at 2θ = 38, 44.2, 64.5, 77.5 and 81.6°, corresponding to the (111), (200), (220), (311) and (422) crystal planes of face-centered-cubic structure of Ag (JCPDS card n°. 04 0783), respectively, indicating the formation of metallic Ag on rGO support. Since diffraction no peaks of copper species were detected, one can assume that these species are highly dispersed over rGO

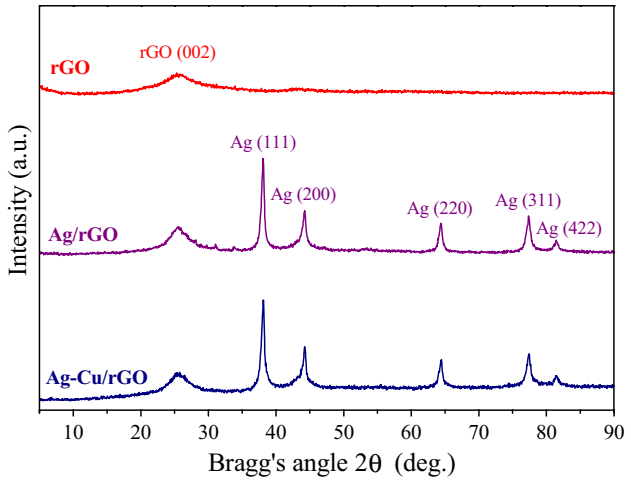

Fig. 1 XRD patterns of rGO, Ag/rGO and Ag–Cu/rGO samples

surface. The crystallite size of Ag on rGO was estimated by the Scherrer equation from the (111) crystalline plane and was found to be around 16 and 17 nm for Ag/rGO and Ag–Cu/rGO catalysts, respectively.

Figure 2 displays the N_2 adsorption–desorption isotherms. As seen, all cases are characterized by type IV isotherms, according to IUPAC classification [44], characteristic of solids containing mesopores. In addition, all hysteresis loops are similar to type-H3, within P/P_0 range of 0.3–0.9, and indicate the formation of mesoporous structures with slit-shaped pores arising from the loose aggregation of sheet-like particle and is common for carbonaceous material [43]. The pronounced hysteresis in case of rGO implies the presence of a more extensively developed pore network. On the other hand, the natural graphite (Fig. S2, SI) exhibited type II isotherms, revealing the no-porous nature of this material.

The textural parameters derived from N_2 physisorption are summarized in Table 1. The results demonstrate that the surface area of rGO increased significantly compared to graphite precursor (from 12 to 481 m^2/g). This increase is attributed to an increasing disorder caused by the oxidative treatment and its subsequently thermal exfoliation at high temperatures [43]. Notably, the rGO prepared in the present work exhibited a high value of BET surface area (481 m^2/g, Table 1), which is comparable to literature [45]. These results are consistent with the XRD analyses. In fact, the rGO has highly porous structure with defects. The textural properties of the Ag/rGO and Ag–Cu/rGO catalysts are presented in Table 1. After impregnation of the metals (Ag and Cu) there is a substantial decrease of the BET surface area (S_{BET}) and of the total pore volume (V_{total}), which can be attributed to the partial pore plugging of rGO mesopores by larger Ag particles (16 and 17 nm).

The thermal stability of the catalysts and of the support under air atmosphere was examined by TGA and the results

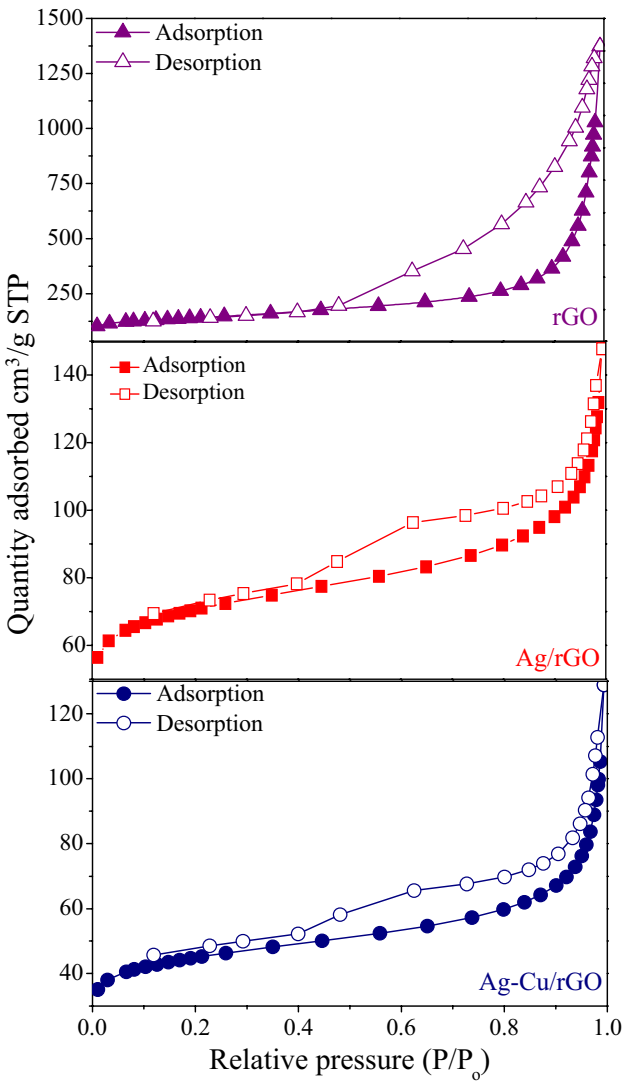

Fig. 2 Nitrogen adsorption–desorption isotherms of the catalysts and support

are shown in Fig. 3. A typical TGA curve of graphene with three events was obtained. The initial weight loss up to 100 °C for rGO is attributed to the removal of adsorbed water. The small weight loss between 150 and 450 °C can be ascribed to the decomposition of the oxygenated functional groups (epoxy, carbonyl, hydroxyl, carboxyl) in the support. It indicates a successful reduction process (functional groups are evidenced by XPS analysis), which are in accordance with XRD measurements and confirm that the functional group inserted in graphite structure was efficiently removed during the reduction process. The weight loss at around 450 °C in rGO is related to the decomposition of carbon skeleton [38]. Similar TGA decomposition profile was obtained for the Ag/rGO catalyst, however the decomposition of the rGO began at lower temperature (around 400 °C) and its total decomposition was reached at 500 °C,

Table 1 Textural properties obtained by N_2 adsorption–desorption measurements

Catalyst	S_{BET} [a] ($m^2\ g^{-1}$)	S_{ext} [b] ($m^2\ g^{-1}$)	V_{total} [c] ($cm^3\ g^{-1}$)	V_{meso} [d] ($cm^3\ g^{-1}$)	D_{BJH} [e] (Å)	Mesoporosity[f] (%)
Graphite	12	8	0.04	0.03	133	75
rGO (support)	481	295	1.42	1.33	107	94
Ag/rGO	239	97	0.19	0.13	64	68
Ag–Cu/rGO	153	66	0.15	0.11	81	73

[a]Derived from the BET model

[b]Derived from the t-plot

[c]Derived from single point measured at $P/P_0 = 0.96$

[d]Determined by total volume minus micropore volume

[e]Desorption average pore diameter

[f]Percentage of V_{meso} to the total pore volume (V_{total})

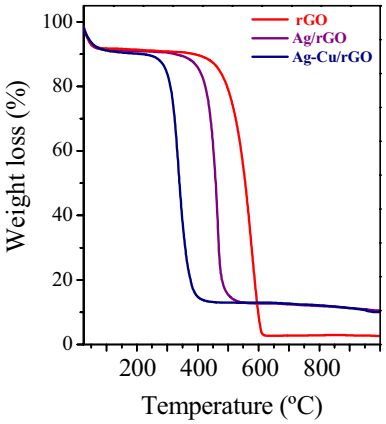

Fig. 3 TGA curves and residual mass of the catalysts and support

a difference of approximately 100 °C below that obtained for pure rGO. In the case of Ag–Cu/rGO catalyst, the decomposition of the rGO carbon began earlier (at 280 °C) and its complete decomposition occurs at 400 °C. According to our results, the decomposition of rGO is much more sensitive in the presence of copper. These results reveal a significant effect of the high dispersed Cu species on the decreasing temperature decomposition of rGO. These observations are in accordance with those reported in the literature [46].

The Ag contents in the Ag/rGO and Ag–Cu/rGO catalysts were determined by TGA results by the weight loss difference between support and catalyst (see Table 2) [47]. The residual mass (a plateaus on the TGA curve) is related to the metal contents in the catalysts. TGA results (Fig. 3) showed that the Ag loading over the rGO support for Ag/rGO and Ag–Cu/rGO catalysts were 9.7 and 9.8 wt%, respectively, which was very close to the targeted nominal value of 10 wt% for Ag. However, copper presents an excess of ~ 5 wt%, which suggests that the rGO decomposes

Table 2 Residual mass

Catalyst	Residual mass after TGA (%)	Ag loadings (wt%)[a]
rGO	2.9	–
Ag/rGO	12.6	9.7
Ag–Cu/rGO	12.8	9.9

[a]Determined by residual mass of catalyst minus residual mass of support

at lower temperature due to the catalytic effect of dispersed Cu on the graphene.

The structural analysis of the catalysts and support were examined by SEM micrographs, as shown in Fig. 4. SEM images reveal that the rGO exhibits a typical morphology with thin sheets structure and highly wrinkled with a few aggregated randomly layers [48]. Generally, in the absence of external forces, the individual sheets prefer to stack to form closed structures in order to decrease the number of dangling bonds and the total energy of the system. The metal particles exhibited a poor distribution on rGO surface and varied sizes for both Ag/rGO and Ag–Cu/rGO catalysts.

EDS elemental mapping confirms the composition and shows the distribution of various elements on the rGO support [29–31]. The elemental distribution map of the Ag/rGO and Ag–Cu/rGO catalysts on the selected area is presented in Figs. S3 (SI) and S4 (SI), respectively. For the Ag/rGO catalyst it is possible verify the existence of domains of Ag, due to its distribution relatively non-uniform. In contrast, the mapping of Ag–Cu/rGO catalyst revealed that Ag and Cu elements are uniformly distributed over graphene sheets. This finding reinforces that Cu is well distributed and was not detected by XRD (Fig. 1). STEM images of catalysts Ag/rGO e Ag–Cu/rGO and EDS elemental mapping of the Ag/rGO are presented in Fig. S5 (SI).

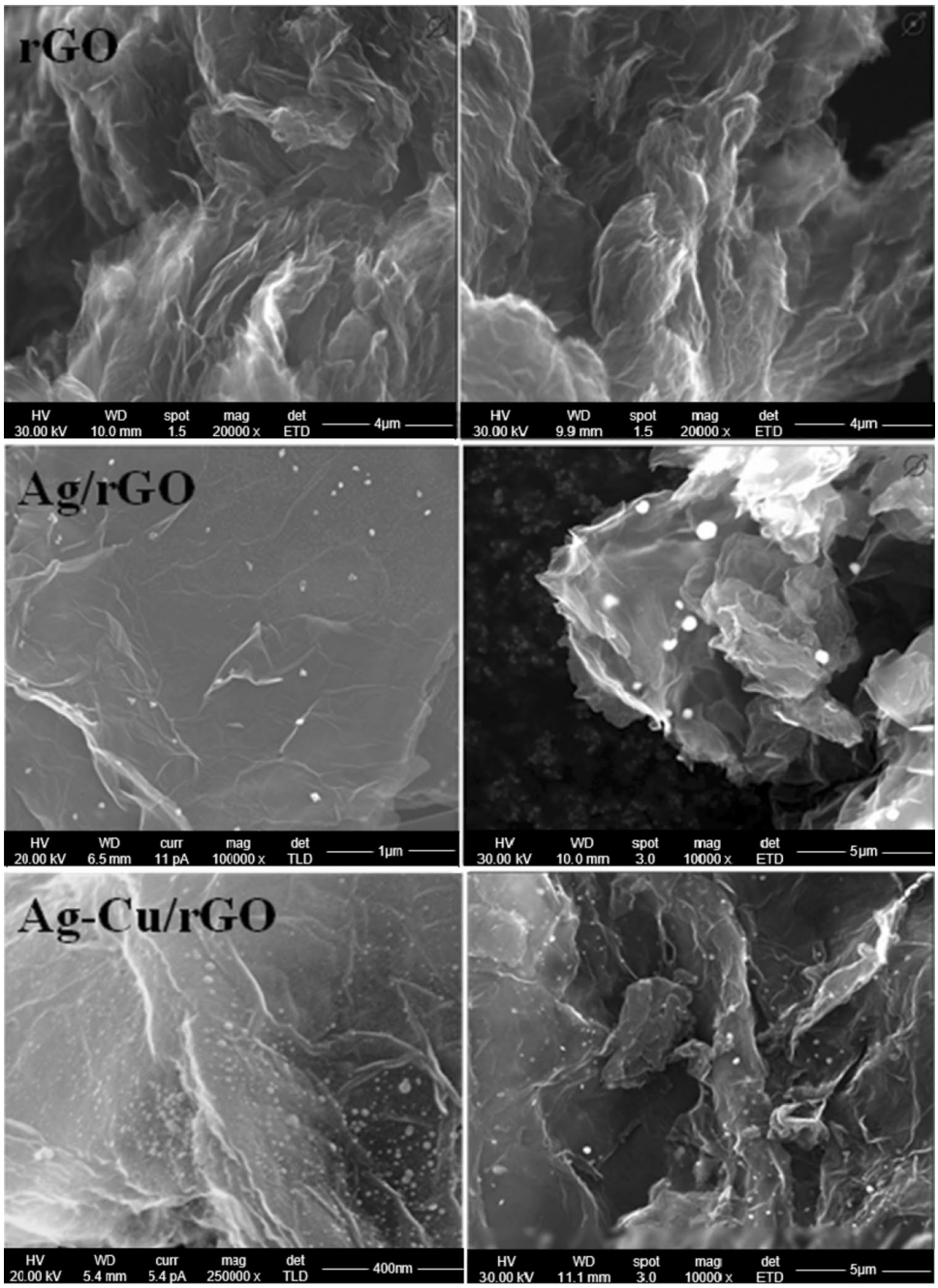

Fig. 4 Representative SEM images of catalysts and support

The surface chemical composition and surface electronic state of the catalysts were evaluated in more details by XPS measurements [29, 30, 40]. The XP spectrum of the rGO is shown in Fig. S6 (SI). As seen, the C1s spectrum was decomposed into four contributions from 280 to 292 eV. The main peak at 284.8 eV was attributed to the sp^2 carbon of the aromatic rings of the rGO structure (C–C/C = C) [49]. Two other components centered at 286.3 and 288.4 eV were associated with C–OH and COOH groups, respectively [49]. They could be attributed to the presence of oxygenated functional groups remaining on rGO surface after reduction of GO, which is consistent with TGA results shown before. The other peak located at 291.2 eV was associated to a satellite peak ($\pi \rightarrow \pi^*$), indicating the delocalized conjugation π, a characteristic of the aromatic carbon structure restored during the reduction [50]. The survey spectrum and the high-resolution XP spectra of Ag 3d, Cu 2p and C 1 s regions for Ag–Cu/rGO catalyst are displayed in Fig. 5. As expected, the survey scan exhibited clearly the predominant peak of carbon (C1s) and a minor (O1s), Ag (3d) and Cu (2p) in the range of 0–1200 eV. No extra peak related with any impurities was detected.

Consistently, two peaks are observed for Ag 3d, with one peak at 368.4 eV corresponding to Ag $3d_{3/2}$ and the other peak at 374.4 eV, associating to Ag $3d_{5/2}$, as expected for metallic Ag [51]. Moreover, the energy difference (ΔE) of the 3d doublet is 6.0 eV (Fig. 5) and confirms the presence of metallic silver in the Ag/rGO catalyst [51]. These findings indicate a similar oxidation state of the atoms on the surface and in the bulk (as evidenced by XRD analysis) and exclude the existence of Ag^{+} and Ag^{2+} species in the Ag–Cu/rGO catalyst. It is noteworthy that both peaks have a small shift toward higher energy level compared to the typical Ag 3d peaks of Ag element, suggesting the interaction between graphene and Ag particles that leads to a decrease in the electron density of Ag atoms, probably due to the conjugation between the d orbital of Ag atom and π bond of graphene [51].

The spectrum relative to the copper exhibited two predominant peaks at 934.2 and 954 eV, which is associating with Cu $2p_{3/2}$ and Cu $2p_{1/2}$, respectively. These binding energies are indicative of the existence of Cu species in the form of bivalent state as CuO [48]. As well, two relatively weak peaks are also observed at approximately 932.4 (Cu $2p_{3/2}$) and 951.9 eV (Cu $2p_{1/2}$), respectively, being attributed to Cu^{+} species as Cu_2O [48]. The XPS results confirm the existence of Cu species (highly dispersed) not detected by XRD analysis (Fig. 1). The spectrum of carbon was fitted using four peaks very similar to the rGO support (Figs. S6, SI). The XP spectra of Ag/rGO catalyst are illustrated in Fig. S7 (SI). No significant differences of these spectra compared to the XP spectra of the Ag–Cu/rGO catalyst (Fig. 5) was observed, except in relation to the presence of copper.

Table 3 summarizes the quantitative analysis of the surface components obtained by XPS analyses. All materials are composed mainly of carbon (79–82 at.%) since it is the main constituent element of graphene's hexagonal network. A significant oxygen amount (17–18 at.%) was also identified on the surface due to residual oxygen groups not removed during the reduction process. The C/O ratios of both catalysts were very similar to those observed for the rGO support. Both catalysts exhibited a similar Ag content (see Table 3), which is lower than the obtained by TGA (bulk analysis), suggesting that metallic Ag is mainly dispersed in the bulk phase. In contrast, the surface copper content of the Ag–Cu/rGO is 1.9 at.%, which suggests the

Table 3 Relative percentages of the different elements on the surface

Catalyst	Surface composition (at.%)				Molar ration
	Ag 3d	Cu 2p	C 1 s	O 1 s	C/O
rGO	–	–	82.3	17.7	4.6
Ag/rGO	0.7	–	81.4	17.9	4.5
Ag–Cu/rGO	0.6	1.9	79.5	17.3	4.6

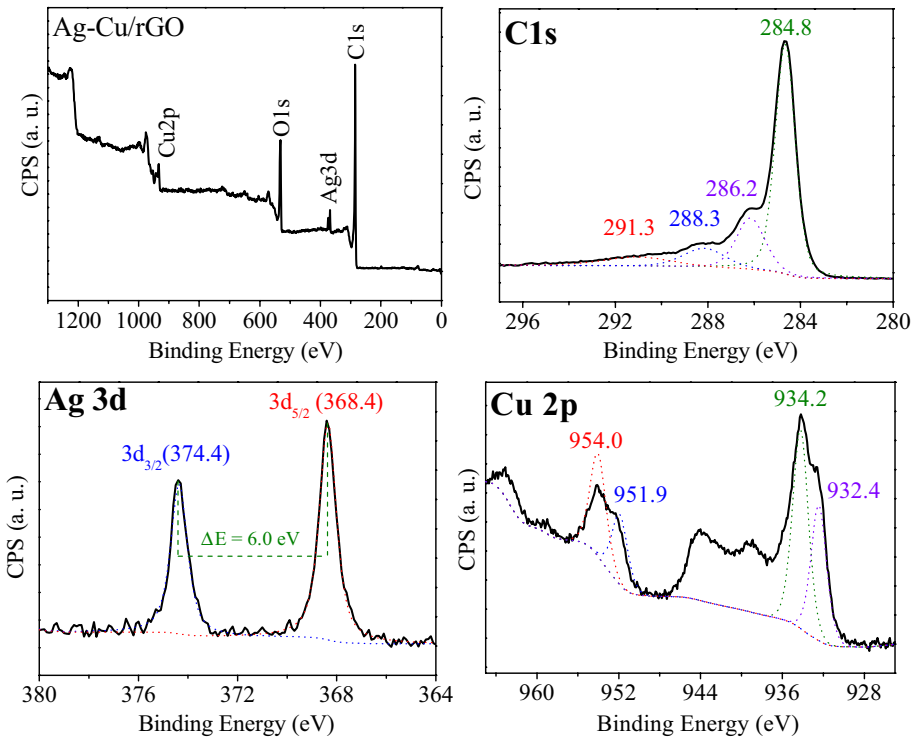

Fig. 5 Survey XP spectrum and high resolution XP spectra of C 1 s, Ag 3d and Cu 2p for Ag–Cu/rGO catalyst

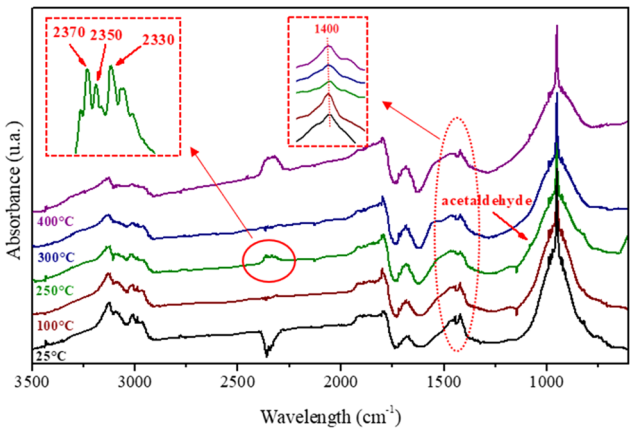

Fig. 6 DRIFT spectra of Ag/rGO catalyst during ethylene oxidation reaction

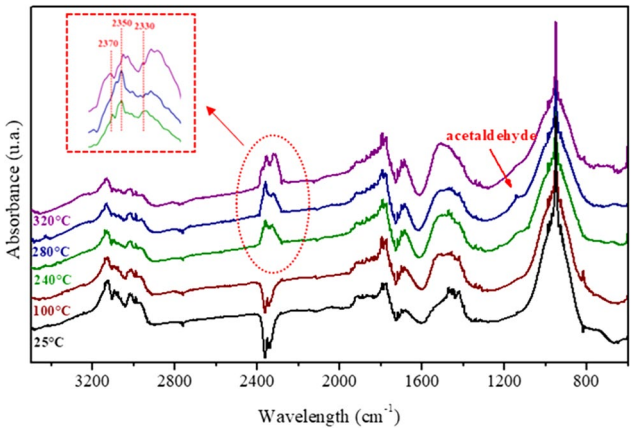

Fig. 7 DRIFT spectra of Ag–Cu/rGO catalyst during ethylene oxidation reaction

Cu species tend to disperse on the surface. This is supported by XRD and EDS analyses.

3.1 In Situ DRIFT Spectroscopy

The in situ DRIFTS experiments were performed with oxygen and reactant mixture ($C_2H_4 + O_2$) on the Ag/rGO and Ag–Cu/rGO catalysts after pretreated at 350 ºC (for Ag/rGO catalyst) and 280 ºC (for Ag–Cu/rGO catalyst), rising the temperature from RT up to 450 ºC (for Ag/rGO catalyst) and 320 ºC (for Ag–Cu/rGO catalyst). Figures 6 and 7 displayed the adsorption bands ascribed to different compounds, according to the literature [52–56].

The reported spectrum for ethylene gas-phase presents a strong band at 900 cm^{-1} due to the H–C–H out of plane wagging, a weak absorption band at 1400 cm^{-1} from H–C–H scissoring and at 3100 cm^{-1}, assigned to the C–H asymmetric stretching [57]. Our spectra showed a strong band at 940 cm^{-1} and weak bands around 3100–2900, 1500–1400 and 1000–890 cm^{-1}. The CO_2 appears between 2370 and 2330 cm^{-1}. One band in the same region of gaseous CO_2 (2350 cm^{-1}) is attributed to CO_2 adsorbed on Ag atoms.

The spectra of Ag/rGO catalyst show that the band corresponding to the ethylene gas-phase at 1400 cm^{-1} that decreases at 250 ºC, appearing new bands at 2370 and 2330 cm^{-1} (corresponding to gaseous CO_2) and at 2350 cm^{-1}, assigned to CO_2 adsorbed on silver oxide. No bands corresponding to the ethylene oxide (1245 cm^{-1}) were observed. The CO_2 bands disappeared at 300 ºC. However, at higher temperature (400 ºC) the CO_2 bands reappeared, indicating the degradation of the support (rGO), in accordance with TGA (Fig. 3) results.

The spectra of the Ag–Cu/rGO catalyst exhibit also the bands assigned to gaseous CO_2 (2370 and 2330 cm^{-1}) and CO_2 adsorbed on silver oxide (2350 cm^{-1}), appearing just at 240 °C. However, with increasing temperature the band of the adsorbed CO_2 decreases, while the band assigned to gaseous CO_2 increases, which indicates degradation of the rGO support, confirming the TGA (Fig. 3) results presented before.

These results indicate that the consumption of ethylene favored the formation of CO_2, which indicates prevailing reaction of total oxidation:

$$C_2H_4 + 3O_2 \rightarrow CO_2 + H_2O$$

However, another band was observed at 1043 cm^{-1} which is assigned to acetaldehyde formation, probably due to the isomerization of ethylene oxide to acetaldehyde, occurring predominantly at the surface of the support and decomposes [27].

According to the literature [10, 35] C_2H_4O can be formed on the hydroxyl containing support and is immediately isomerized to acetaldehyde. According to the FTIR analysis (Fig. 8), the rGO has oxygenated functional groups in its structure.

The infrared spectrum of the rGO showed a broad and intense band between 2900 and 3600 cm^{-1} attributed to the stretching vibrations of the OH group. In this band there would be superposed OH groups of alcohols, phenols, carboxylic acids. Carboxylic acids are also represented by a small band at 1730 cm^{-1} associated with the stretching of the C = O bond. Another band around 1400 cm^{-1} is due to the angular deformation in the OH connection plane. The band at 1230 cm^{-1} represents the stretching modes of the epoxide group (C–O–C), while the band at 1050 cm^{-1} is characteristic of vibrations of the alkoxide group (C–O) [58].

According to the literature [10, 35] C_2H_4O can be formed on the hydroxyl containing support and is

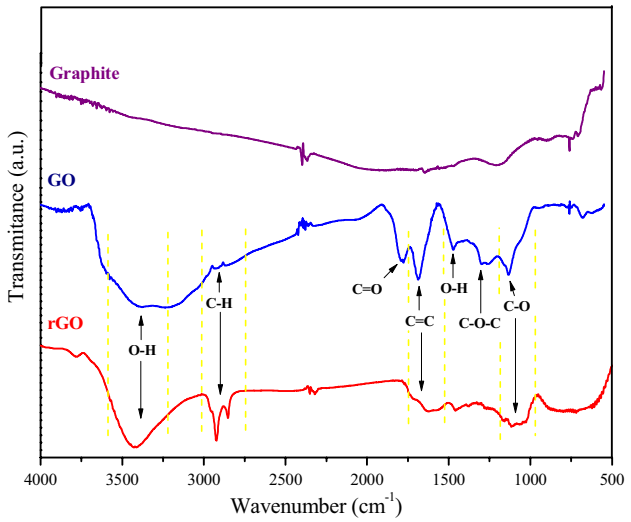

Fig. 8 FTIR spectra of graphite, GO and rGO

immediately isomerized to acetaldehyde. It seems that the oxidation of ethylene enables the formation of the intermediate acetaldehyde and suggests that if any ethylene oxide was formed can quickly be isomerized to acetaldehyde since the rGO contains functional groups at the surface.

Ethylene reacts with hydroxyls and [O] present on the surface of the support from the rGO synthesis process, resulting in acetaldehyde as a product. This acetaldehyde is decomposed to CO_2 and H_2O, products of the total oxidation of ethylene.

$$C_2H_4 + [OH] \rightarrow H_2O + 2C + 2H_2$$

$$C_2H_4 + {}^1/_2\,O_2 \rightarrow CH_3CHO \rightarrow 2CO_2 + 2H_2O$$

$$C_2H_4 + [O] \rightarrow CH_3CHO \rightarrow CO_2 + H_2O$$

It seems that the oxidation of ethylene enables the formation of the intermediate acetaldehyde and suggests that if any ethylene oxide was formed can quickly be isomerized to acetaldehyde since the rGO contains functional groups at the surface.

The literature reported high selectivity to ethylene oxide on Ag supported on alumina and promoted by Cs with low contents that affects the surface properties of the support. In general, Ag supported on silica or alumina present poor activity and high selectivity [33]. The literature affirm that the metallic Ag is responsible for the epoxidation reaction. Since graphene is an inert material the metal should be responsible for the epoxidation reaction. However, XPS results showed that there are isolated or dispersed ionic Cu species on graphene and over the metallic Ag. Therefore, the dispersed Cu ion species indicate the influence of electronic structure on the reaction, and according the in situ DRIFTS results enhances the total oxidation reaction with intermediate acetaldehyde formation and then total oxidation and not the partial oxidation reaction. It seems that to favor the partial oxidation the support plays an important role. In fact, our previous work for Ag/Al_2O_3 showed through DRIFTS results the preferential partial oxidation reaction, confirming our proposal.

There are possible scenarios for depicting the role of Ag and with the addition of Cu for the epoxidation reaction. According to Kokalj et al. [59], there is a stronger O surface bonding to the C surface bond. The transition state of the intermediate to acetaldehyde is stronger on the Cu–O than on the C-Cu bond, favoring the epoxide. The O-Ag bond presents lower barrier to aldehyde and thus favor the epoxide selectivity. In the Ag–Cu/rGO system the oxygen atom of the intermediate oxametallacycle intermediate is bound on both Ag and Cu, and the C atom of this intermediate specie bond only to Ag. On the other hand, since Cu is dispersed over the surface or coated as segregated phases Cu_2O/CuO, while Ag are isolated atoms, it favors the total oxidation, because during the decomposition of C_2H_4 into C and H, these C are linked to the Cu species, while the dissociated O_2 over the metallic Ag particles. The reaction occurs preferentially between the C and the molecular oxygen and due to the poorer dispersion of Cu species on bigger Ag particles the epoxidation reaction is not favored, which explains the lower activation.

It seems that the reaction mechanism on Ag and Ag–Cu on graphene are different, because the O_2 dissociation barrier and activation energy for ethylene transformation are lower for the Ag–Cu than on Ag. Therefore, the adsorption on Ag–Cu supported on graphene indicate intermediate species of ethylene adsorbed on Cu species and not on Ag, as evidenced by IR spectra, through the presence of ethylene oxide, acetaldehyde and CO_2.

From these results we can suggest two possible surface mechanism (Scheme 1). One, assuming that ethylene is dissociated on Cu species, with the formation of C, that reacts with the molecular oxygen, favoring the total oxidation and that Ag is not active. The second possibility, is that besides the dissociation of ethylene on Cu species, the oxygen dissociates at the surface of Ag particles and since Cu species are dispersed on Ag particles, it is that the dissociated oxygen can react with the ethylene intermediate species, like ethylidene species, as suggested by Somorjai et al. [60] favoring the epoxidation reaction with the formation of ethylene oxide at temperatures between 200 and 280 ºC. Therefore, Cu can promote the epoxidation due to the higher dispersion on Ag surface over the graphene. Moreover, graphene is inert and dispersed well the Cu species at the surface, not interacting with Ag. Bigger Ag particles on graphene favor the total oxidation. Indeed,

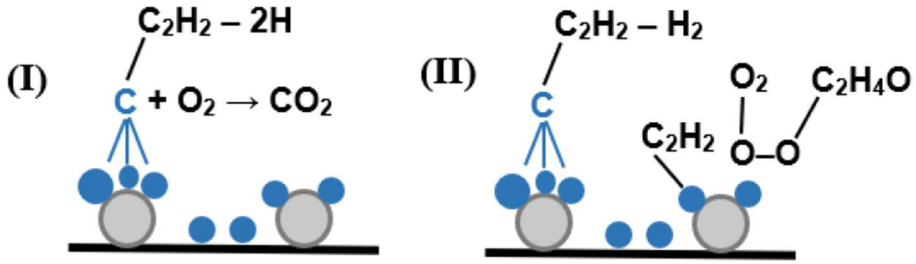

Scheme 1 Possible reaction mechanisms of ethylene oxidation at the surface of Ag/rGO and Ag–Cu/RGO catalysts

additional experimental work is necessary to identify the structure giving rise to these spectroscopic results.

4 Conclusion

Defects are observed in the regular hexagonal structure of the graphene sheet after the oxidation process of graphite and exfoliation and reduction of graphite oxide. Wet impregnation proved to be an efficient method for the preparation of the silver and silver–copper supported in the rGO. The metals were dispersed and varied in size on the rGO surface. XPS results showed the presence of the metallic silver and the copper as the CuO and Cu_2O oxides, being CuO as major content. The presence of the metals on the surface of the rGO reduced its thermal stability in the presence of O_2. The in situ DRIFTS results showed total oxidation of ethylene and intermediate formation of acetaldehyde that is decomposed. The presence of Cu ions or CuO and Cu_2O at the surface indicate the presence of electronic structure, which may enhance the oxidation reaction and the total oxidation.

Acknowledgements The authors acknowledge FAPERJ for scholarships; Surface Chemistry Laboratory—LAQUIS (IQ/UFRJ) for the XPS analysis; Characterization Center in Nanotechnology for Materials and Catalysis (CENANO/INT) for the SEM analysis.

References

1. Greiner MT et al (2015) The oxidation of copper catalysts during ethylene epoxidation. Phys Chem Chem Phys 17(38):25073–25089
2. Li CJ, Bi X (2018) Silver catalysis in organic synthesis, 1st edn. Wiley, New York
3. Lefort TE (1931) Fr. Patent 729:952; Lefort TE (1935) US Patent 1:998
4. Pu T, Tian H, Ford ME, Rangarajan S, Wachs IE (2019) Overview of selective oxidation of ethylene to ethylene oxide by Ag catalysts. ACS Catal 12(9):10727–10750
5. Ozbek MO, Onal I, Van Santen RA (2011) Why silver is the unique catalyst for ethylene epoxidation. J Catal 284(2):230–235
6. Jankowiak JT, Barteau MA (2005) Ethylene epoxidation over silver and copper-silver bimetallic catalysts: I. Kinetics and selectivity. J Catal 236(2):366–378
7. Greiner M et al (2018) Phase coexistence of multiple copper oxides on AgCu catalysts during ethylene epoxidation. ACS Catal 8(3):2286–2295
8. Zhan T, Zhang Y, Liu X, Lu S, Hou W (2016) NiFe layered double hydroxide/reduced graphene oxide nanohybrid as an efficient bifunctional electrocatalyst for oxygen evolution and reduction reactions. J Power Sources 333:53–60
9. Pendashteh A, Palma J, Anderson M, Marcilla R (2017) $NiCoMnO_4$ nanoparticles on N-doped graphene: Highly efficient bifunctional electrocatalyst for oxygen reduction/evolution reactions. Appl Catal B 201:241–252
10. Xiong H, Jewell LL, Coville NJ (2015) Shaped carbons as supports for the catalytic conversion of syngas to clean fuels. ACS Catal 5(4):2640–2658
11. Cheng Y, Lin J, Xu K, Wang H, Yao X, Pei Y, Yan S, Qiao M, Zong B (2016) Fischer−Tropsch synthesis to lower olefins over potassium-promoted reduced graphene oxide supported iron catalysts. ACS Catal 6(1):389–399
12. Low J, Yu J, Ho W (2015) Graphene-based photocatalysts for CO_2 reduction to solar fuel. J Phys Chem Lett 6(21):4244–4251
13. Li F, Zhang L, Tong J, Liu Y, Xu S, Cao Y, Cao S (2016) Photocatalytic CO_2 conversion to methanol by Cu_2O/graphene/TNA heterostructure catalyst in a visible-light-driven dual-chamber reactor. Nano Energy 27:320–329
14. Geng J, Kuai L, Kan E, Sang Y, Geng B (2016) Hydrothermal synthesis of a rGO nanosheet enwrapped NiFe nanoalloy for superior electrocatalytic oxygen evolution reactions. Chemistry A 22(41):14480–14483
15. Mateo D, Esteve-Adell I, Albero J, Primo A, García H (2017) Oriented 2.0.0 Cu_2O nanoplatelets supported on few-layers graphene as efficient visible light photocatalyst for overall water splitting. Appl Catal B 201:582–590
16. Chen F, Surkus AE, He L, Pohl MM, Radnik J, Topf C, Junge K, Beller M (2015) Selective catalytic hydrogenation of heteroarenes with N-graphene-modified cobalt nanoparticles (Co_3O_4-Co/NGratα-Al_2O_3). J Am Chem Soc 137(36):11718–11724
17. Nie R, Miao M, Du W, Shi J, Liu Y, Hou Z (2016) Selective hydrogenation of CC bond over N-doped reduced graphene oxides supported Pd catalyst. Appl Catal B 180:607–613
18. Zheng J, Duan X, Lin H, Gu Z, Fang H, Li J, Yuan Y (2016) Silver nanoparticles confined in carbon nanotubes: on the understanding of the confinement effect and promotional catalysis for the selective hydrogenation of dimethyl oxalate. Nanoscale 8(11):5959–5967
19. Lu X, Song C, Jia S, Tong Z, Tang X, Teng Y (2015) Low-temperature selective catalytic reduction of NO_x with NH_3 over cerium and manganese oxides supported on TiO_2-graphene. Chem Eng J 260:776–784
20. Xiao X, Sheng Z, Yang L, Dong F (2016) Low-temperature selective catalytic reduction of NO_x with NH_3 over a manganese and cerium oxide/graphene composite prepared by a hydrothermal method. Catal Sci Technol 6(5):1507–1514

21. Trapalis A, Todorova N, Giannakopoulou T, Boukos N, Speliotis T, Dimotikali D, Yu J (2016) TiO_2/graphene composite photocatalysts for NO_x removal: a comparison of surfactant-stabilized graphene and reduced graphene oxide. Appl Catal B 180:637–647
22. Hu M, Yao Z, Hui KN, Hui KS (2017) Novel mechanistic view of catalytic ozonation of gaseous toluene by dual-site kinetic modelling. Chem Eng J 308:710–718
23. Hu M, Hui KS, Hui KN (2014) Role of graphene in MnO_2/graphene composite for catalytic ozonation of gaseous toluene. Chem Eng J 254:237–244
24. Chavez-Sumarriva I, Van Steenberge PHM, D'Hooge DR (2016) New insights in the treatment of waste water with graphene: dual-site adsorption by sodium dodecylbenzenesulfonate. Ind Eng Chem Res 55(35):9387–9396
25. Ramakrishnan S, Karuppannan M, Vinothkannan M, Ramachandran K, Joong Kwon O, Jin Yoo D (2019) Ultrafine Pt nanoparticles stabilized by MoS_2/N-doped reduced graphene oxide as a durable electrocatalyst for alcohol oxidation and oxygen reduction reactions. ACS Appl Mater Interfaces 11:12504–12515
26. Hu M, Yao Z, Wang X (2017) Graphene-based nanomaterials for catalysis. Ind Eng Chem Res 56(13):3477–3502
27. Huang C, Li C, Shi G (2012) Graphene based catalysts. Energy Environ Sci 5(10):8848
28. Edwards RS, Coleman KS (2013) Graphene synthesis: relationship to applications. Nanoscale 5(1):38–51
29. Meng HB, Zhang XF, Pu YL, Chen XL, Feng JJ, Han DM, Wang AJ (2019) One-pot solvothermal synthesis of reduced graphene oxide-supported uniform PtCo nanocrystals for efficient and robust electrocatalysis. J Colloid Interface Sci 543:17–24
30. Shi YC, Feng JJ, Lin Pu XX, Zhang L, Yuan J, Zhang QL, Wang AJ (2019) One-step hydrothermal synthesis of three-dimensional nitrogen-doped reduced graphene oxide hydrogels anchored ptpd alloyed nanoparticles for ethylene glycol oxidation and hydrogen evolution reactions. Electrochim Acta 293:504–513
31. Chen HY, Niu HJ, Ma X, Feng JJ, Weng X, Huang H, Wang AJ (2020) Flower-like platinum-cobalt-ruthenium alloy nanoassemblies as robust and highly efficient electrocatalyst for hydrogen evolution reaction. J Colloid Interface Sci 561:372–378
32. Deng D, Novoselov KS, Fu Q, Zheng N, Tian Z, Bao X (2016) Catalysis with two-dimensional materials and their heterostructures. Nat Nanotechnol 11(3):218–230
33. Cheng Y, Zhao Q, Li Y, Peng W, Zhang G, Zhang F, Fan X (2016) Gold nanoparticles supported on layered TiO_2-RGO hybrid as an enhanced and recyclable catalyst for microwave-assisted hydration reaction. RSC Adv 6(80):76151–76157
34. Dey A, Athar J, Varma P, Prasant H, Sikder AK, Chattopadhyay S (2015) Graphene-iron oxide nanocomposite (GINC): An efficient catalyst for ammonium perchlorate (AP) decomposition and burn rate enhancer for AP based composite propellant. RSC Adv 5(3):1950–1960
35. Bai S, Shen X (2012) Graphene–inorganic nanocomposites. RSC Adv 2(1):64–98
36. Zhang N, Zhang Y, Xu YJ (2012) Recent progress on graphene-based photocatalysts: current status and future perspectives. Nanoscale 4(19):5792–5813
37. Chen J, Yao B, Li C, Shi G (2013) An improved Hummers method for eco-friendly synthesis of graphene oxide. Carbon N Y 64:225–229
38. Zhang G, Wen M, Wang S, Chen J, Wang J (2018) Insights into thermal reduction of the oxidized graphite from the electro-oxidation processing of nuclear graphite matrix. RSC Adv 567(8):567–572
39. Amorim de Carvalho MCN, Passos FB, Schmal M (2007) Study of the active phase of silver catalysts for ethylene epoxidation. J Catal 248(1):124–129
40. Zhang RL, Duan JJ, Han Z, Feng JJ, Huang H, Zhang QL, Wang AJ (2020) One-step aqueous synthesis of hierarchically multi-branched PdRuCu nanoassemblies with highly boosted catalytic activity for ethanol and ethylene glycol oxidation reactions. Appl Surf Sci 506:144791
41. Miller TS, Jorge AB, Suter TM, Sella A, Cora F, McMillan PF (2017) Carbon nitrides: synthesis and characterization of a new class of functional materials. Phys Chem Chem Phys 19:15613–15638
42. Dehghanzad B, Aghjeh MKR, Rafeie O, Tavakolic A, Oskooieab AJ (2016) Synthesis and characterization of graphene and functionalized graphene via chemical and thermal treatment methods. RSC Adv 6:3578–3585
43. Abdolhosseinzadeh S, Asgharzadeh H, Kim HS (2015) Fast and fully-scalable synthesis of reduced graphene oxide. Sci Rep 5(1):1–7
44. Condon JB (2006) Surface area and porosity determinations by physisorption. Elsevier Science, Amsterdam1
45. Stankovich S, Dikin DA, Piner RD, Kohlhaas KA, Kleinhammes A, Jia Y, Wu Y, Nguyen ST, Ruoff RS (2007) Synthesis of graphene-based nanosheets via chemical reduction of exfoliated graphite oxide. Carbon 45(7):1558–1565
46. Zhao Y, Song X, Song Q, Yin Z (2012) A facile route to the synthesis copper oxide/reduced graphene oxide nanocomposites and electrochemical detection of catechol organic pollutant. CrystEngComm 14(20):6710
47. Kumar A et al (2017) Greener route for synthesis of aryl and alkyl-14H-dibenzo [a.j] xanthenes using graphene oxide-copper ferrite nanocomposite as a recyclable heterogeneous catalyst. Sci Rep 7:1–18
48. Zheng X et al (2012) Epoxidation of propylene by molecular oxygen over supported Ag-Cu bimetallic catalysts with low Ag loading. J Mol Catal A 357:106–111
49. Xu C, Shi X, Ji A, Shi L, Zhou C, Cui Y (2015) Fabrication and characteristics of reduced graphene oxide produced with different green reductants. PLoS ONE 10(12):1–15
50. Ganguly A et al (2011) Probing the thermal deoxygenation of graphene oxide using high-resolution in situ X-ray-based spectroscopies. J Phys Chem C 115(34):17009–17019
51. Bukhtiyarov VI, Nizovskii AI, Bluhm H, Hävecker M, Kleimenov E, Knop-Gericke A, Schlögl R (2006) Combined in situ XPS and PTRMS study of ethylene epoxidation over silver. J Catal 238(2):260–269
52. Goncharova SN, Paukshtis EA, Bal'zhinimaevoncharova BS (1995) Size effects in ethylene oxidation on silver catalysts: influence of support and Cs promoter. Appl Catal A 126(1):67–84
53. Tsybula SV, Kryukova GN, Goncharova SN, Shmakov AN, Bal'zhinimaevoncharova BS (1995) Study of the real structure of silver supported catalysts of different dispersity. J Catal 154(2):194–200
54. Force EL, Bell AT (1975) Infrared spectra of adsorbed species present during the oxidation of ethylene over silver. J Catal 38(1):440–460
55. Force EL, Bell AT (1975) The relationship of adsorbed species observed by infrared spectroscopy to the mechanism of ethylene oxidation over silver. J Catal 40(3):356–371
56. Kilty PA, Sachtler WMH (1974) The mechanism of the selective oxidation of ethylene to ethylene oxide. Catal Rev Sci Eng 10:1–16
57. Alpert NL, Keiser WE, Szymanski HA (1970) The use of characteristic group frequencies in structural analysis, 1st edn. Springer, New York1

58. Mathkar A, Tozier D, Cox P, Ong P, Galande C, Balakrishnan K, Reddy ALM, Ajayan PM (2012) Controlled, stepwise reduction and band gap manipulation of graphene oxide. J Phys Chem Lett 3(8):986–991
59. Kokalj A, Gava P, Gironcoli S, Baroni S (2008) What determines the catalyst's selectivity in the ethylene epoxidation reaction. J Catal 254(2):304–309
60. Cremer PS, Stanners C, Niemantsverdriet JW, Shen YR, Somorjai G (1995) The conversion of di-σ bonded ethylene to ethylidyne on Pt(111) monitored with sum frequency generation: evidence for an ethylidene (or ethyl) intermediate. Surf Sci 328(1):111–118

Affiliations

Monique R. D'Oliveira[1] · Jessica Rabelo[1] · Amanda Garcez Veiga[2] · Carlos Alberto Chagas[3] · Martin Schmal[1,4]

✉ Martin Schmal
schmal@peq.coppe.ufrj.br

[1] Nanotechnology Engineering Program, COPPE, Federal University of Rio de Janeiro, Rio de Janeiro, RJ 21941-972, Brazil

[2] Insitute of Chemistry, Federal University of Rio de Janeiro, Rio de Janeiro, RJ 21941-909, Brazil

[3] School of Chemistry, Federal University of Rio de Janeiro, Rio de Janeiro, RJ 21941-909, Brazil

[4] Chemical Engineering Program, COPPE, Federal University of Rio de Janeiro, Rio de Janeiro, RJ 21941-914, Brazil